Coupled Systems Mechanics, *Vol. 6, No. 4 (2017) 417-437*
DOI: https://doi.org/10.12989/csm.2017.6.4.417

A comparative study for design of boundary combined footings of trapezoidal and rectangular forms using new models

Arnulfo Luévanos-Rojas[*1], José Daniel Barquero-Cabrero[2a], Sandra López-Chavarría[1b] and Manuel Medina-Elizondo[1c]

[1]Institute of Multidisciplinary Researches, Autonomous University of Coahuila, Blvd. Revolución No, 151 Ote, CP 27000, Torreón, Coahuila, México
[2]Institute for Long Life Learning IL3, University of Barcelona, Street Girona No, 24, CP 08010, Barcelona, Spain

(Received April 27, 2017, Revised August 23, 2017, Accepted August 24, 2017)

Abstract. This paper shows a comparative study for design of reinforced concrete boundary combined footings of trapezoidal and rectangular forms supporting two columns and each column transmits an axial load and a moment around of the axis X (transverse axis of the footing) and other moment around of the axis Y (longitudinal axis of the footing) to foundation to obtain the most economical combined footing. The real soil pressure acting on the contact surface of the footings is assumed as a linear variation. Methodology used to obtain the dimensions of the footings for the two models consider that the axis X of the footing is located in the same position of the resultant, i.e., the dimensions is obtained from the position of the resultant. The main part of this research is to present the differences between the two models. Results show that the trapezoidal combined footing is more economical compared to the rectangular combined footing. Therefore, the new model for the design of trapezoidal combined footings should be used, and complies with real conditions.

Keywords: design of trapezoidal combined footings; design of rectangular combined footings; bending moments; bending shear; punching shear

1. Introduction

Footings are structural elements that transmit column or wall loads to the underlying soil below the structure. Footings are designed to transmit these loads to the soil without exceeding its safe bearing capacity, to prevent excessive settlement of the structure to a tolerable limit, to minimize differential settlement, and to prevent sliding and overturning. The choice of suitable type of

∗Corresponding author, Ph.D., E-mail: arnulfol_2007@hotmail.com
[a]Ph.D., E-mail: jd.barquero@eserp.com
[b]Ph.D., E-mail: sandylopez5@hotmail.com
[c]Ph.D., E-mail: drmanuelmediana@yahoo.com.mx

footing depends on the depth at which the bearing stratum is localized, the soil condition and the type of superstructure. The foundations are classified into superficial and deep, which have important differences: in terms of geometry, the behavior of the soil, its structural functionality and its constructive systems (Bowles 2001, Das *et al.* 2006).

The design of superficial solution is done for the following load cases: 1) the footings subjected to concentric axial load, 2) the footings subjected to axial load and moment in one direction (uniaxial bending), 3) the footings subjected to axial load and moment in two directions (biaxial bending) (Bowles 2001, Das *et al.* 2006, Calabera 2000, Tomlinson 2008, McCormac and Brown 2013, González-Cuevas and Robles-Fernandez-Villegas 2005).

Superficial foundations may be of various types according to their function; isolated footing, combined footing, strip footing, or mat foundation (Bowles 2001).

A combined footing is a long footing supporting two or more columns in (typically two) one row. The combined footing may be rectangular, trapezoidal or T-shaped in plan. Rectangular footing is provided when one of the projections of the footing is restricted or the width of the footing is restricted. Trapezoidal footing or T-shaped is provided when one column load is much more than the other. As a result, both projections of the footing beyond the faces of the columns will be restricted (Kurian 2005, Punmia *et al.* 2007, Varghese 2009).

The distribution of soil pressure under a footing is a function of the type of soil, the relative rigidity of the soil and the footing, and the depth of foundation at level of contact between footing and soil. A concrete footing on sand will have a pressure distribution similar to Fig. 1(a). A concrete footing on clay will have a pressure distribution similar to Fig. 1(b). As the footing is loaded, the soil under the footing deflects in a bowl-shaped depression, relieving the pressure under the middle of the footing. For design purposes, it is common to assume the soil pressure is linearly distributed. The pressure distribution will be uniform if the centroid of the footing coincides with the resultant of the applied loads, as shown in Fig. 1(c) (Bowles 2001).

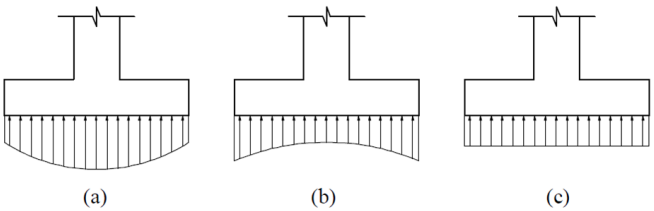

Fig. 1 Pressure distribution under footing; (a) footing on sand; (b) footing on clay; (c) equivalent uniform distribution

Construction practice may dictate using only one footing for two or more columns due to:

a) Closeness of column (for example around elevator shafts and escalators).

b) To property line constraint, this may limit the size of footings at boundary. The eccentricity of a column placed on an edge of a footing may be compensated by tying the footing to the interior column.

Conventional method for design of combined footings by rigid method assumes that (Bowles 2001, Das *et al*. 2006, McCormac and Brown 2013, González-Cuevas and Robles-Fernandez-Villegas 2005):

1. The footing or mat is infinitely rigid, and therefore, the deflection of the footing or mat does

not influence the pressure distribution.

2. The soil pressure is linearly distributed or the pressure distribution will be uniform, if the centroid of the footing coincides with the resultant of the applied loads acting on foundations.

3. The minimum stress should be equal to or greater than zero, because the soil is not capable of withstand tensile stresses.

4. The maximum stress must be equal or less than the allowable capacity that can withstand the soil.

Some papers presents the equations to obtain the dimension of footings are: A mathematical model for dimensioning of rectangular footings (Luévanos-Rojas 2013); A mathematical model for dimensioning of square footings (Luévanos-Rojas 2012a); A mathematical model for the dimensioning of circular footings (Luévanos-Rojas 2012b); A new mathematical model for dimensioning of the boundary trapezoidal combined footings (Luévanos-Rojas 2015a); A mathematical model for the dimensioning of rectangular combined footings (Luévanos-Rojas 2016a); Optimal dimensioning for the corner combined footings (López-Chavarría *et al.* 2017).

Guler and Celep (2005) presented the response of a rectangular plate-column system on a tensionless winkler foundation subjected to static and dynamic loads.

Chen *et al.* (2011) investigated the nonlinear vibration behavior for a hybrid composite plate subjected to initial stresses on elastic foundations to obtain the nonlinear partial differential equations of motion.

Smith-Pardo (2011) showed a study on a performance-based framework for soil-structure systems using simplified rocking foundation models.

Shahin and Cheung (2011) presented the stochastic design charts for bearing capacity of strip footings.

Zhang *et al.* (2011) showed a nonlinear analysis of finite beam resting on winkler with consideration of beam-soil interface resistance effect.

Agrawal and Hora (2012) presented a nonlinear interaction behavior of infilled frame-isolated footings-soil system subjected to seismic loading.

Rad (2012) realized the study on the static behavior of bi-directional functionally graded (FG) non-uniform thickness circular plate resting on quadratically gradient elastic foundations (Winkler-Pasternak type) subjected to axisymmetric transverse and in-plane shear efforts is carried out by using a model 3D and differential quadrature methods.

Maheshwari and Khatri (2012) estimated the influence of inclusion of geosynthetic layer on response of combined footings on stone column of earth beds reinforced.

Orbanich *et al.* (2012) showed a study on strenghtening and repair of concrete foundation beams with fiber composite materials.

Mohamed *et al*. (2013) presented the generalized schmertmann equation for settlement estimation of shallow footings in saturated and unsaturated sands.

Luévanos-Rojas *et al.* (2013) proposed a design of isolated footings of rectangular form using a new model.

Orbanich and Ortega (2013) this study aimed to investigate the mechanical behavior of rectangular foundation plates with perimetric beams and internal stiffening beams of the plate is herein analyzed, taking the foundation design into account.

Dixit and Patil (2013) showed an experimental estimate of $N\gamma$ values and corresponding settlements for square footings on finite layer of sand.

ErzÍn and Gul (2013) presented the use of neural networks for the prediction of the settlement of pad footings on cohesionless soils based on standard penetration test.

Cure *et al*. (2014) proposed the decrease trends of ultimate loads of eccentrically loaded model strip footings close to a slope.

Luévanos-Rojas (2014a) presented a design of isolated footings of circular form using a new model.

Luévanos-Rojas (2014b) proposed a design of boundary combined footings of rectangular shape using a new model.

Uncuoğlu (2015) showed a study on bearing capacity of square footings on sand layer overlying clay.

Luévanos-Rojas (2015b) presented a design of boundary combined footings of trapezoidal form using a new model.

Luévanos-Rojas (2016b) showed a comparative study for the design of rectangular and circular isolated footings using new models.

Luévanos-Rojas (2016c) proposed a new model for design of boundary rectangular combined footings with two opposite sides restricted.

This paper shows a comparative study for design of reinforced concrete boundary combined footings of trapezoidal and rectangular forms supporting two columns and each column transmits an axial load and a moment around of the axis X (transverse axis of the footing) and other moment around of the axis Y (longitudinal axis of the footing) to foundation to obtain the most economical combined footing. The real soil pressure acting on the contact surface of the footings is assumed as a linear variation. Methodology used to obtain the dimensions of the footings for the two models consider that the axis X of the footing is located in the same position of the resultant, i.e., the dimensions of the footings is obtained from the position of the resultant. The main part of this research is to present the differences between the two models.

2. Formulation of the new models

2.1 Boundary trapezoidal combined footings

Fig. 2 shows a boundary trapezoidal combined footing supporting two rectangular columns of different dimensions (one boundary column and other inner column) subjected to axial load and moments in two directions in each column.

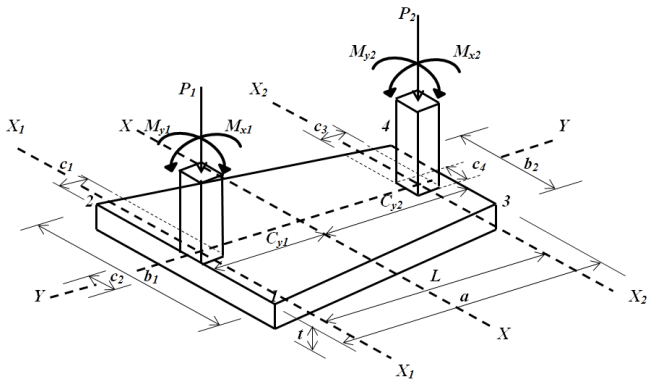

Fig. 2 Trapezoidal combined footing with one property line

The value of "C_{y1}" is obtained by the equation (Luévanos-Rojas 2015a)

$$C_{y1} = \frac{Rc_1 + 2P_2L - 2M_{xT}}{2R} \tag{1}$$

where: $R=P_1+P_2$ and $M_{xT}=M_{x1}+M_{x2}$.

The value of "a" must comply with the following (Luévanos-Rojas 2015a)

$$\frac{3}{2}C_{y1} < a < 3C_{y1} \tag{2}$$

If the trapezoidal combined footing has two property lines in opposite ends. The value of "a" is (Luévanos-Rojas 2015a)

$$a = \frac{c_1}{2} + L + \frac{c_3}{2} \tag{3}$$

The value of "b_2" is found as follows. If the soil pressure is considered equal to zero, the value of "b_2" is obtained by the following equation (Luévanos-Rojas 2015a)

$$b_2 = \frac{12M_{yT}(2a - 3C_{y1})(3C_{y1} - a)}{R(5a^2 - 18aC_{y1} + 18{C_{y1}}^2)} \tag{4}$$

where: $M_{yT}=M_{y1}+M_{y2}$.

Now, if the soil pressure is considered available load capacity "σ_{adm}", the value of "b_2" is obtained by the following equation (Luévanos-Rojas 2015a)

$$\begin{aligned}\sigma_{adm}a^2(5a^2 - 18aC_{y1} + 18{C_{y1}}^2){b_2}^2 - 2R(3C_{y1} - a)(5a^2 - 18aC_{y1} + 18{C_{y1}}^2)b_2 \\ - 24M_{yT}(2a - 3C_{y1})(3C_{y1} - a)^2 = 0\end{aligned} \tag{5}$$

The greater value obtained by Eqs. (4)-(5) is the value considered for "b_2".

Once known the value of "b_2" is substituted into following equation to obtain the value of "b_1" (Luévanos-Rojas 2015a)

$$b_1 = \left(\frac{2a - 3C_{y1}}{3C_{y1} - a}\right)b_2 \tag{6}$$

2.1.1 Moments

Critical sections for moments are presented in section a_1'-a_1', a_2'-a_2', b'-b', c'-c', d'-d' and e'-e', as shown in Fig. 3.

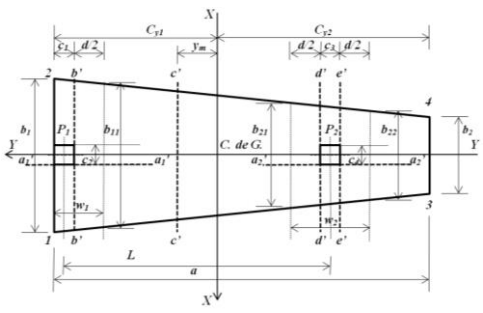

Fig. 3 Critical sections for moments

2.1.1.1 Moment around of the axis a_1'-a_1'

The moment around of the axis a_1'-a_1' is obtained using the following equation (Luévanos-Rojas 2015b)

$$M_{a_1} = \left[P_1 a\left(b_1{}^2 + b_{11}{}^2\right)\{3a^2(b_1-c_2)^2 - 3aw_1(b_1-b_2)(b_1-c_2) + w_1{}^2(b_1-b_2)^2\}\right.$$
$$+ 6M_{y1}\{2a^3\left(2b_1{}^3 - 3b_1{}^2c_2 + c_2{}^3\right) - 6a^2b_1w_1(b_1-b_2)(b_1-c_2)$$
$$\left. + 2aw_1{}^2(b_1-b_2)^2(2b_1-c_2) - w_1{}^3(b_1-b_2)^3\}\right] \quad (7)$$
$$/\left[12a^3(b_1+b_{11})\left(b_1{}^2+b_{11}{}^2\right)\right]$$

2.1.1.2 Moment around of the axis a_2'-a_2'

The moment around of the axis a_2'-a_2' is obtained using the following equation (Luévanos-Rojas 2015b)

$$M_{a_2} = \left[P_2 a\left(b_{21}{}^2 + b_{22}{}^2\right)\{3[2a(b_1-c_4) - (b_1-b_2)(2L+c_1)]^2 + w_2{}^2(b_1-b_2)^2\}\right.$$
$$+ 12M_{y2}\{4a^3(b_1-c_4)^2(2b_1+c_4) - 12a^2b_1(b_1-c_4)(b_1-b_2)(2L+c_1)$$
$$+ a(b_1-b_2)^2(2b_1-c_4)[3(2L+c_1)^2 + w_2{}^2]$$
$$\left. - (b_1-b_2)^3[(2L+c_1)^3 + w_2{}^2(2L+c_1)]\}\right] \quad (8)$$
$$/\left[48a^3(b_{21}+b_{22})\left(b_{21}{}^2+b_{22}{}^2\right)\right]$$

where: $w_1 = c_1+d/2$, $w_2 = c_3+d$, $b_{11} = b_1 - w_1(b_1-b_2)/a$, $b_{21} = b_1 - (c_1+2L-w_2)(b_1-b_2)/2a$, $b_{22} = b_1 - (c_1+2L+w_2)(b_1-b_2)/2a$.

2.1.1.3 Moment around of the axis b'-b'

The moment around of the axis b'-b' is (Luévanos-Rojas 2015b)

$$M_b = \frac{P_1c_1}{2} - \frac{Rc_1{}^2[3ab_1 - c_1(b_1-b_2)]}{3a^2(b_1+b_2)} + M_{x1} \quad (9)$$

2.1.1.4 Moment around of the axis c'-c'

The maximum moment is presented on the axis c'-c', and shear force is zero. Then the shear force is obtained at a distance "y_m", and must be equal to zero. The equation to obtain "y_m" is shown as follows (Luévanos-Rojas 2015b)

$$y_m = \frac{a\sqrt{R\left[b_1{}^2(R-P_1) + P_1b_2{}^2\right]} - R\left(C_{y1}b_2 + C_{y2}b_1\right)}{R(b_1-b_2)} \quad (10)$$

The moment around of the axis c'-c' is obtained using the following equation (Luévanos-Rojas 2015b)

$$M_c = P_1\left(C_{y1} - \frac{c_1}{2} - y_m\right) - \frac{R\left(C_{y1}-y_m\right)\left[2ab_2 + (b_1-b_2)\left(2C_{y2}+C_{y1}+y_m\right)\right](y_{cc}-y_m)}{a^2(b_1+b_2)} \quad (11)$$
$$+ M_{x1}$$

where: y_{cc} is the gravity center of the soil pressure the area formed by the axis *c'-c'* and the corners 1 and 2 with respect the axis "*X*", and this is obtained by the following equation (Luévanos-Rojas 2015b)

$$y_{cc} = \frac{(b_1 - b_2)(C_{y1} - y_m)^2}{6[2ab_2 + (b_1 - b_2)(2C_{y2} + C_{y1} + y_m)]} + \frac{C_{y1}}{2} + \frac{y_m}{2} \tag{12}$$

2.1.1.5 Moment around of the axis d'-d'

The moment around of the axis *d'-d'* is obtained using the following equation (Luévanos-Rojas 2015b)

$$M_d = P_1\left(L - \frac{c_3}{2}\right) - \frac{R(2L - c_3 + c_1)^2[6ab_1 - (b_1 - b_2)(2L - c_3 + c_1)]}{24a^2(b_1 + b_2)} + M_{x1} \tag{13}$$

2.1.1.6 Moment around of the axis e'-e'

The moment around of the axis *e'-e'* is obtained as follows (Luévanos-Rojas 2015b)

$$M_e = P_1\left(L + \frac{c_3}{2}\right) + P_2\left(\frac{c_3}{2}\right) - \frac{R(2L + c_3 + c_1)^2[6ab_1 - (b_1 - b_2)(2L + c_3 + c_1)]}{24a^2(b_1 + b_2)} + M_{x1} + M_{x2} \tag{14}$$

2.1.2 Bending shear (unidirectional shear force)

Critical sections for bending shear are obtained at a distance "*d*" starting the junction of the column with the footing as seen in Fig. 4, these are presented in sections f_1'-f_1', f_2'-f_2', *g'-g'*, *h'-h'* and *i'-i'*.

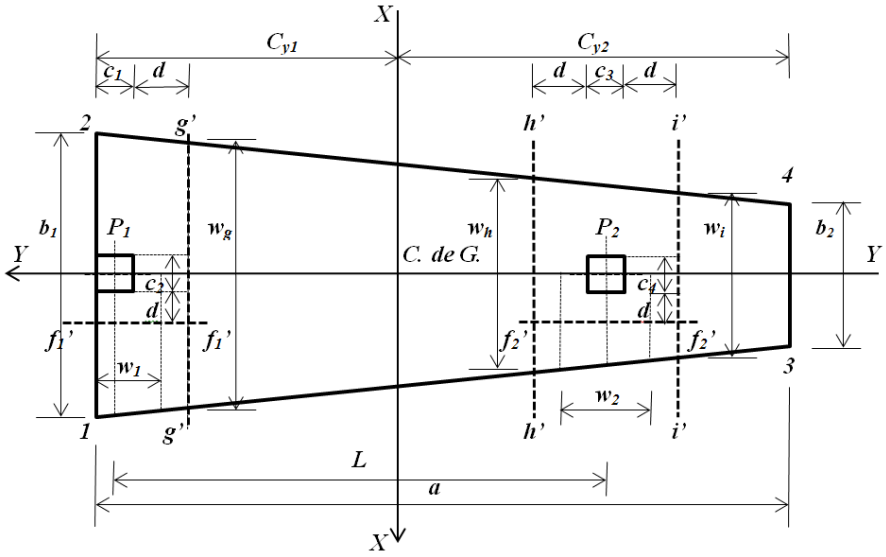

Fig. 4 Critical sections for bending shear

2.1.2.1 Bending shear on the axis f_1'-f_1'

Bending shear acting on the axis f_1'-f_1' of the footing "V_{ff1}" is obtained through the pressure volume of the area formed by the axis f_1'-f_1' with a width "$w_1 = c_1+d/2$" and the free end of the footing, where the greatest pressure is presented (Luévanos-Rojas 2015b)

$$V_{ff_1} = \left[P_1 a\left(b_1{}^2 + b_{11}{}^2\right)[2a(b_1 - c_2 - 2d) - w_1(b_1 - b_2)]\right.$$
$$\left. + 4M_{y1}\{3a^2\left[b_1{}^2 - (c_2 + 2d)^2\right] - 3ab_1w_1(b_1 - b_2) + w_1{}^2(b_1 - b_2)^2\}\right]$$
$$/2a^2(b_1 + b_{11})\left(b_1{}^2 + b_{11}{}^2\right) \tag{15}$$

2.1.2.2 Bending shear on the axis f_2'-f_2'

Bending shear acting on the axis f_2'-f_2' of the footing "V_{ff2}" is obtained through the pressure volume of the area formed by the axis f_2'-f_2' with a width "$w_2 = c_3+d$" and the free end of the footing, where the greatest pressure is obtained (Luévanos-Rojas 2015b)

$$V_{ff_2} = \left[P_2 a\left(b_{21}{}^2 + b_{22}{}^2\right)[2a(b_1 - c_4 - 2d) - (b_1 - b_2)(2L + c_1)]\right.$$
$$+ M_{y2}\{3[2ab_1 - (b_1 - b_2)(2L + c_1)]^2 - 12a^2(c_4 + 2d)^2$$
$$\left. + w_2{}^2(b_1 - b_2)^2\}\right]/\left[2a^2(b_{21} + b_{22})\left(b_{21}{}^2 + b_{22}{}^2\right)\right] \tag{16}$$

2.1.2.3 Bending shear on the axis g'-g'

Bending shear acting on the axis g'-g' of the footing "V_{fg}" is the force "P_1" acting on column 1 subtracting the pressure volume of the area formed by the axis g'-g' and the corners 1 and 2, which is found to the left of the footing, this is as follows (Luévanos-Rojas 2015b)

$$V_{fg} = P_1 - \frac{R(c_1 + d)[2ab_1 - (b_1 - b_2)(c_1 + d)]}{a^2(b_1 + b_2)} \tag{17}$$

2.1.2.4 Bending shear on axis h'-h'

Bending shear acting on the axis h'-h' of the footing "V_{fh}" is the force "P_1" acting on column 1 subtracting the pressure volume of the area formed by the axis h'-h' and the corners 1 and 2, which is found to the left of the footing, this is as follows (Luévanos-Rojas 2015b)

$$V_{fh} = P_1 - \frac{R(2L + c_1 - c_3 - 2d)[4ab_1 - (b_1 - b_2)(2L + c_1 - c_3 - 2d)]}{4a^2(b_1 + b_2)} \tag{18}$$

2.1.2.5 Bending shear on axis i'-i'

Bending shear acting on the axis i'-i' of the footing "V_{fi}" is the sum of the force "P_1" acting on column 1 and the force "P_2" acting on column 2 subtracting the pressure volume of the area formed by the axis i'-i' and the corners 1 and 2, which is found to the left of the footing, this is (Luévanos-Rojas 2015b)

$$V_{fi} = R - \frac{R(2L + c_1 + c_3 + 2d)[4ab_1 - (b_1 - b_2)(2L + c_1 + c_3 + 2d)]}{4a^2(b_1 + b_2)} \tag{19}$$

2.1.3 Punching shear (bidirectional shear force)

Critical section for the punching shear appears at a distance "*d*/2" starting the junction of the column with the footing in the two directions, as shown in Fig. 5.

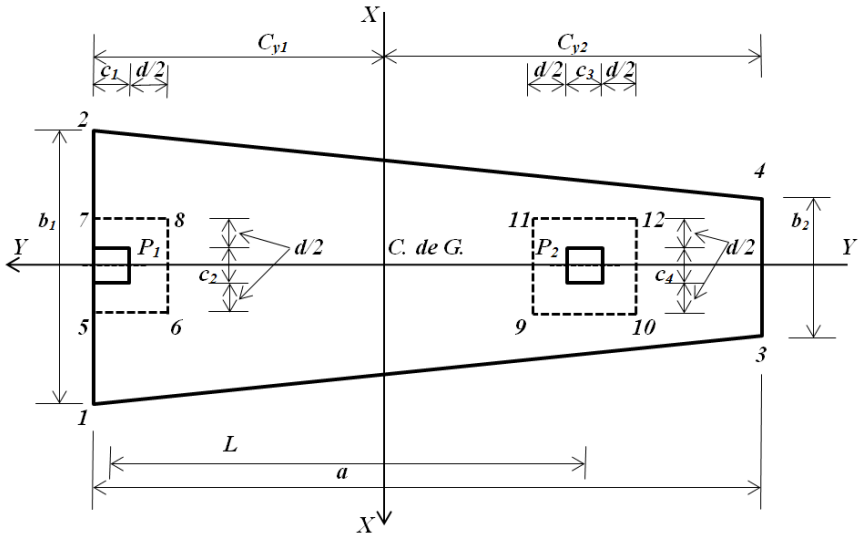

Fig. 5 Critical sections for punching shear

2.1.3.1 Punching shear for boundary column

Critical section for the punching shear is presented in rectangular section formed by points 5, 6, 7 and 8. Punching shear acting on the footing "V_{p1}" is the force "P_1" acting on column 1 subtracting the pressure volume of the area formed by point's 5, 6, 7 and 8 (Luévanos-Rojas 2015b)

$$V_{p1} = P_1 - \frac{R(2c_1 + d)(c_2 + d)}{a(b_1 + b_2)} \tag{20}$$

2.1.3.2 Punching shear for inner column

Critical section for the punching shear is presented in rectangular section formed by points 9, 10, 11 and 12. Punching shear acting on the footing "V_{p2}" is the force "P_2" acting on column 2 subtracting the pressure volume of the area formed by the point's 9, 10, 11 and 12 (Luévanos-Rojas 2015b)

$$V_{p2} = P_2 - \frac{2R(c_3 + d)(c_4 + d)}{a(b_1 + b_2)} \tag{21}$$

2.2 Boundary rectangular combined footings

Fig. 6 shows a combined footing supporting two rectangular columns of different dimensions (a boundary column and other inner column) subject to axial load and moments in two directions (bidirectional bending) each column.

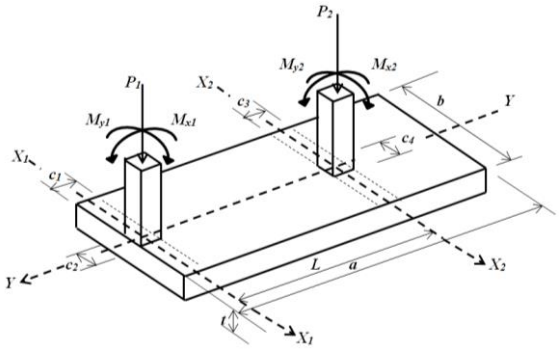

Fig. 6 Rectangular combined footing with one property line

The value of "*a*" is selected according to the following equation (Luévanos-Rojas 2016a)

$$a = 2\left(\frac{c_1}{2} + \frac{P_2 L - M_{xT}}{R}\right) \tag{22}$$

where: *a* is the dimension of the footing in the direction parallel to the axis "*Y*", *R* is the sum of the forces of $P_1 + P_2$ (Resultant force), M_{xT} is the sum of moments around the axis "*X*" of $M_{x1}+M_{x2}$.

The value of "*b*" is found as follows. If the soil pressure is considered equal to zero, the value of "*b*" is obtained by the following equation (Luévanos-Rojas 2016a)

$$b = \frac{6M_{yT}}{R} \tag{23}$$

where: $M_{yT} = M_{y1} + M_{y2}$.

Now, if the soil pressure is considered available load capacity "σ_{adm}", the value of "*b*" is obtained by the following equation (Luévanos-Rojas 2016a)

$$b = \frac{R + \sqrt{R^2 + 24\sigma_{adm} a M_{yT}}}{2\sigma_{adm} a} \tag{24}$$

The greater value obtained by Eqs. (23)-(24) is the value considered for "*b*".

2.2.1 Moments

Critical sections for moments are presented in section *a₁'-a₁'*, *a₂'-a₂'*, *b'-b'*, *c'-c'*, *d'-d'* and *e'-e'*, as shown in Fig. 7.

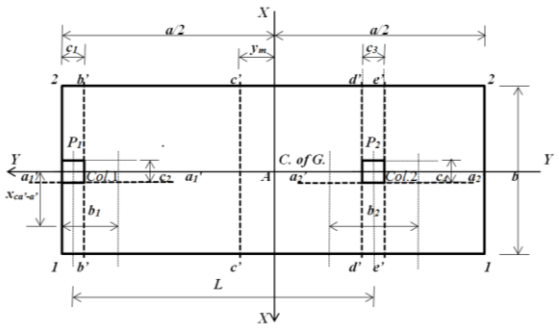

Fig. 7 Critical sections for moments

2.2.1.1 Moment around of the axis a₁'-a₁'

The moment around of the axis a_1'-a_1' is obtained using the following equation (Luévanos-Rojas 2014b)

$$M_{a_1} = \frac{(b-c_2)^2\left[P_1 b^2 + 2M_{y1}(2b+c_2)\right]}{8b^3} \tag{25}$$

2.2.1.2 Moment around of the axis a₂'-a₂'

The moment around of the axis a_2'-a_2' is obtained using the following equation (Luévanos-Rojas 2014b)

$$M_{a_2} = \frac{(b-c_4)^2\left[P_2 b^2 + 2M_{y2}(2b+c_4)\right]}{8b^3} \tag{26}$$

2.2.1.3 Moment around of the axis b'-b'

The moment around of the axis *b'-b'* is obtained using the following equation (Luévanos-Rojas 2014b)

$$M_b = \left(P_1 - \frac{Rc_1}{a}\right)\frac{c_1}{2} + M_{x1} \tag{27}$$

2.2.1.4 Moment around of the axis c'-c'

The maximum moment is presented on the axis *c'-c'*, and shear force is zero. Then the shear force is obtained at a distance "y_m", and must be equal to zero. The equation to obtain "y_m" is shown as follows (Luévanos-Rojas 2014b)

$$y_m = \frac{a}{2} - \frac{P_1 a}{R} \tag{28}$$

The moment around of the axis *c'-c'* is obtained using the following equation (Luévanos-Rojas 2014b)

$$M_c = \frac{P_1(P_1 a - Rc_1)}{2R} + M_{x1} \tag{29}$$

2.2.1.5 Moment around of the axis d'-d'

The moment around of the axis *d'-d'* is obtained using the following equation (Luévanos-Rojas 2014b)

$$M_d = P_1\left(L - \frac{c_3}{2}\right) - \frac{R}{2a}\left(L + \frac{c_1 - c_3}{2}\right)^2 + M_{x1} \tag{30}$$

2.2.1.6 Moment around of the axis e'-e'

The moment around of the axis *e'-e'* is obtained using the following equation (Luévanos-Rojas 2014b)

$$M_e = P_1 L + \frac{Rc_3}{2} - \frac{R}{2a}\left(L + \frac{c_1 + c_3}{2}\right)^2 + M_{x1} + M_{x2} \tag{31}$$

2.2.2 Bending shear (unidirectional shear force)

The critical sections for bending shear are obtained at a distance "*d*" starting the junction of the column with the footing as seen in Fig. 8, these are presented in sections f_1'-f_1', f_2'-f_2', g'-g', h'-h' and i'-i'.

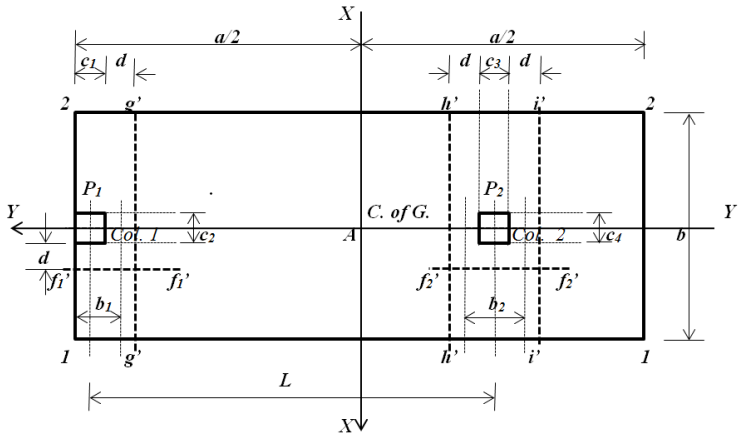

Fig. 8 Critical sections for bending shear

2.2.2.1 Bending shear on the axis f_1'-f_1'

Bending shear acting on the axis f_1'-f_1' of the footing "V_{ff1}" is obtained through of the volume of pressure of the area formed by the axis f_1'-f_1' with a width "$b_1 = c_1+d/2$" and the free end of the rectangular footing, where the greatest pressure is presented (Luévanos-Rojas 2014b)

$$V_{ff_1} = \frac{P_1(b - c_2 - 2d)}{2b} + \frac{3M_{y1}[b^2 - (c_2 + 2d)^2]}{2b^3} \tag{32}$$

2.2.2.2 Bending shear on the axis f_2'-f_2'

Bending shear acting on the axis f_2'-f_2' of the footing "V_{ff2}" is obtained through of the volume of pressure of the area formed by the axis f_2'-f_2' with a width "$b_2 = c_3+d$" and the free end of the rectangular footing, where the greatest pressure is presented (Luévanos-Rojas 2014b)

$$V_{ff_2} = \frac{P_2(b - c_4 - 2d)}{2b} + \frac{3M_{y2}[b^2 - (c_4 + 2d)^2]}{2b^3} \tag{33}$$

2.2.2.3 Bending shear on the axis g'-g'

Bending shear acting on the axis g'-g' of the footing "V_{fg}" is obtained through of the volume of pressure of the area formed by the axis g'-g' and the corners 1 and 2 to the left of the footing, this is as follows (Luévanos-Rojas 2014b)

$$V_{fg'} = P_1 - \frac{R(c_1 + d)}{a} \tag{34}$$

2.2.2.4 Bending shear on the axis h'-h'

Bending shear acting on the axis *h*'-*h*' of the footing "V_{fh}" is the force "P_1" acting in column 1 less the volume of pressure of the area formed by the axis *h*'-*h*' and the corners 1 and 2, which is found to the left of the footing, this is as follows (Luévanos-Rojas 2014b)

$$V_{fh'} = P_1 - \frac{R}{a}\left(L + \frac{c_1 - c_3}{2} - d\right) \tag{35}$$

2.2.2.5 Bending shear on the axis i'-i'

Bending shear acting on the axis *i*'-*i*' of the footing "V_{fi}" is the sum of the force "P_1" acting on column 1 and the force "P_2" acting on column 2 less the volume of pressure of the area formed by the axis *i*'-*i*' and the corners 1 and 2, which is found to the left of the footing, this is as follows (Luévanos-Rojas 2014b)

$$V_{fi'} = R - \frac{R}{a}\left(L + \frac{c_1 + c_3}{2} + d\right) \tag{36}$$

2.2.3 Punching shear (bidirectional shear force)

The critical section for the punching shear appears at a distance "*d*/2" starting the junction of the column with the footing in the two directions, as shown in Fig. 9.

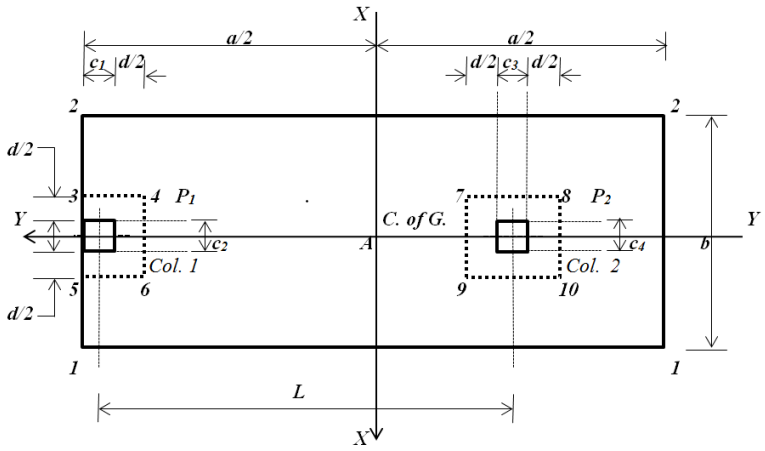

Fig. 9 Critical sections for punching shear

2.2.3.1 Punching shear for boundary column

The critical section for the punching shear is presented in rectangular section formed by points 3, 4, 5 and 6. Punching shear acting on the footing "V_{p1}" is the force "P_1" acting on column 1 subtracting the pressure volume of the area formed by the point's 3, 4, 5 and 6 (Luévanos-Rojas 2014b)

$$V_{p1} = P_1 - \frac{R(c_1 + d/2)(c_2 + d)}{ab} \tag{37}$$

2.2.3.2 Punching shear for inner column

The critical section for the punching shear is presented in rectangular section formed by points 7, 8, 9 and 10. Punching shear acting on the footing "V_{p2}" is the force "P_2" acting on column 2 subtracting the pressure volume of the area formed by the point's 7, 8, 9 and 10 (Luévanos-Rojas 2014b)

$$V_{p2} = P_2 - \frac{R(c_3 + d)(c_4 + d)}{ab} \tag{38}$$

3. Numerical problems

The design of two boundary combined footings of trapezoidal and rectangular form using new models supporting two square columns are shown and the general information for the two cases is: column 1 is of 40×40 *cm*; column 2 is of 40×40 *cm*; *L* is the center-to-center distance between the two columns = 6.00 *m*; *H* is the depth of the footing = 1.5 *m*; f'_c is the specified compressive strength of concrete at 28 days = 21 *MPa*; f_y is the specified yield strength of reinforcement of steel = 420 *MPa*; q_a is the allowable load capacity of the soil = 220 kN/m^2; γ_{ppz} is the self-weight of the footing = 24 kN/m^3; γ_{pps} is the self-weight of soil fill = 15 kN/m^3.

Table 1 presents the mechanical elements acting on the footing for two cases different.

Table 1 Mechanical elements acting on the footing

Case	Loads of the column 1						Loads of the column 2					
	Dead load			Live load			Dead load			Live load		
	P_{D1} kN	M_{Dx1} kN-m	M_{Dy1} kN-m	P_{L1} kN	M_{Lx1} kN-m	M_{Ly1} kN-m	P_{D2} kN	M_{Dx2} kN-m	M_{Dy2} kN-m	P_{L2} kN	M_{Lx2} kN-m	M_{Ly2} kN-m
1	700	140	120	500	100	80	1400	280	240	1000	200	160
2	700	0	0	500	0	0	1400	0	0	1000	0	0

The nomenclature used in the Tables 2 and 3 are as follows:

TCF_1 = Trapezoidal Combined Footing of the type 1, TCF_2 = Trapezoidal Combined Footing of the type 2, TCF_3 = Trapezoidal Combined Footing of the type 3, RCF = Rectangular Combined Footing, MF = Measures of the footings, M_{a1} = Moment acting around of the axis a_1-a_1 (*kN-m*), M_{a2} = Moment acting around of the axis a_2-a_2 (*kN-m*), M_b = Moment acting around of the axis *b-b* (*kN-m*), M_c = Moment acting around of the axis *c-c* (*kN-m*), M_d = Moment acting around of the axis *d-d* (*kN-m*), M_e = Moment acting around of the axis *e-e* (*kN-m*), $Ø_vV_{ff1}$ = Bending shear resisted by the concrete on the axis f_1-f_1 (*kN*), V_{ff1} = Bending shear acting on the axis f_1-f_1 (*kN*), $Ø_vV_{ff2}$ = Bending shear resisted by the concrete on the axis f_2-f_2 (*kN*), V_{ff2} = Bending shear acting on the axis f_2-f_2 (*kN*), $Ø_vV_{fg}$ = Bending shear resisted by the concrete on the axis *g-g* (*kN*), V_{fg} = Bending shear acting on the axis *g-g* (*kN*), $Ø_vV_{fh}$ = Bending shear resisted by the concrete on the axis *h-h* (*kN*), V_{fh} = Bending shear acting on the axis *h-h* (*kN*), $Ø_vV_{fi}$ = Bending shear resisted by the concrete on the axis *i-i* (*kN*), V_{fi} = Bending shear acting on the axis *i-i* (*kN*), $Ø_vV_{cp11}$ = Punching shear resisted by the concrete (Column 1) (*kN*), $Ø_vV_{cp12}$ = Punching shear resisted by the concrete (Column 1) (*kN*), $Ø_vV_{cp13}$ = Punching shear resisted by the concrete (Column 1) (*kN*), V_{p1}

= Punching shear acting on the Column 1 (*kN*), $Ø_vV_{cp21}$ = Punching shear resisted by the concrete (Column 2) (*kN*), $Ø_vV_{cp22}$ = Punching shear resisted by the concrete (Column 2) (*kN*), $Ø_vV_{cp23}$ = Punching shear resisted by the concrete (Column 2) (*kN*), V_{p2} = Punching shear acting on the Column 2 (*kN*), d = Effective depth (*cm*), t = Total thickness (*cm*), V_C = Volume of concrete (m^3), V_{sty} = Volume of reinforcement steel in direction of the axis "Y" at the top of the footing (cm^3), V_{sby} = Volume of reinforcement steel in direction of the axis "Y" at the bottom of the footing (cm^3), V_{sTy} = Volume of total reinforcement steel in direction of the axis "Y" of the footing (cm^3), V_{stx} = Volume of reinforcement steel in direction of the axis "X" at the top of the footing (cm^3), V_{sbx} = Volume of reinforcement steel in direction of the axis "X" at the bottom of the footing (cm^3), V_{sTx} = Volume of total reinforcement steel in direction of the axis "X" of the footing (cm^3), $V_{sT} = V_{sTy} + V_{sTx}$ = Total volume of the reinforcement steel of the footing (cm^3).

Bending shear (unidirectional shear force) resisted by the concrete *"V_{cf}"* is given (ACI 318-14)

$$Ø_vV_{cf} = 0.17Ø_v\sqrt{f'_c}b_wd \tag{39}$$

where: $Ø_v$ is the strength reduction factor by shear is 0.85, b_w is the width where the bending shear is presented.

The width b_w for the trapezoidal combined footings in anywhere is obtained

$$b_w = b_1 - y(b_1 - b_2)/a \tag{40}$$

where: y is the distance from of the largest width to the axis under study.

Punching shear (shear force bidirectional) resisted by the concrete "V_{cp}" is given (ACI 318-14)

$$Ø_vV_{cp1} = 0.17Ø_v\left(1 + \frac{2}{\beta_c}\right)\sqrt{f'_c}b_0d \tag{41a}$$

where: β_c is the ratio of long side to short side of the column and b_0 is the perimeter of the critical section.

$$Ø_vV_{cp2} = 0.083Ø_v\left(\frac{\alpha_s d}{b_0} + 2\right)\sqrt{f'_c}b_0d \tag{41b}$$

where: α_s is 40 for interior columns, 30 for edge columns, and 20 for corner columns.

$$Ø_vV_{cp3} = 0.33Ø_v\sqrt{f'_c}b_0d \tag{41c}$$

where: $Ø_vV_{cp}$ must be the value smallest of Eqs (41*a*)-(41*b*)-(41*c*).

Tables 2 and 3 show the solution for three different types of dimensions for the combined trapezoidal footings, because the value of "*a*" is restricted according to Eq. (2), and for the combined rectangular footings is proposed one type of dimensions.

Table 2 shows the solution for the case 1.

Table 2 Comparison of results to the case 1

Concept	TCF_1	TCF_2	TCF_3	RCF	Relationship 1	Relationship 2	Relationship 3
MF	a = 7.00 b_1 = 1.80 b_2 = 4.50	a = 7.50 b_1 = 2.55 b_2 = 3.80	a = 8.50 b_1 = 3.65 b_2 = 2.55	a = 8.00 b = 3.20	RCF/TCF_1	RCF/TCF_2	RCF/TCF_3
M_{a1}	353.20	491.67	695.47	612.88	1.74	1.25	0.88
M_{a2}	1639.90	1388.32	1076.72	1225.77	0.75	0.88	1.14

Table 2 Continued

M_b	622.95	613.48	601.74	606.80	0.97	0.99	1.01
M_c	2724.39	2408.84	2032.70	2186.67	0.80	0.91	1.08
M_d	-487.70	-883.28	-1557.44	-1230.00	2.52	1.39	0.79
M_e	-117.64	-486.74	-1093.77	-787.20	6.69	1.62	0.72
$Ø_vV_{ff1}$	568.45	523.92	439.82	481.04	0.85	0.92	1.09
V_{ff1}	0	161.56	431.57	342.10	∞	2.12	0.79
$Ø_vV_{ff2}$	879.97	804.15	662.45	731.65	0.83	0.91	1.10
V_{ff2}	857.17	754.44	603.86	684.21	0.80	0.91	1.13
$Ø_vV_{fg}$	1496.60	1687.51	1895.03	1843.52	1.23	1.09	0.97
V_{fg}	1009.00	914.54	826.53	858.95	0.85	0.94	1.04
$Ø_vV_{fh}$	2402.26	2071.31	1618.11	1843.52	0.77	0.89	1.14
V_{fh}	-1468.96	-1480.81	-1566.08	-1514.95	1.03	1.02	0.97
$Ø_vV_{fi}$	2980.35	2296.71	1476.93	1843.52	0.62	0.80	1.25
V_{fi}	0	140.77	629.24	448.95	∞	3.19	0.71
$Ø_vV_{cp11}$	6050.62	5555.97	4626.27	5081.19	0.84	0.91	1.10
$Ø_vV_{cp12}$	11095.23	10017.67	8027.43	8995.07	0.81	0.90	1.12
$Ø_vV_{cp13}$	3915.11	3595.04	2993.47	3287.83	0.84	0.91	1.10
V_{p1}	1369.47	1405.45	1455.49	1436.19	1.05	1.02	0.99
$Ø_vV_{cp21}$	10559.69	9649.85	7949.36	8779.74	0.83	0.91	1.10
$Ø_vV_{cp22}$	15604.82	14086.60	11282.94	12645.97	0.81	0.90	1.12
$Ø_vV_{cp23}$	6832.74	6244.02	5143.71	5681.01	0.83	0.91	1.10
V_{p2}	2861.21	2920.00	3002.09	2970.02	1.04	1.02	0.99
d	97	92	82	87	0.90	0.95	1.06
t	105	100	90	95	0.90	0.95	1.06
V_C	23.15	23.81	23.71	24.32	1.05	1.02	1.03
V_{sty}	71263.92	75707.77	72442.70	77064.00	1.08	1.02	1.06
V_{sby}	73428.81	74833.20	74468.16	77064.00	1.05	1.03	1.03
V_{sTy}	144692.73	150540.97	146910.32	154128.00	1.07	1.02	1.05
V_{stx}	42490.35	42760.13	42705.60	44083.20	1.04	1.03	1.03
V_{sbx}	53183.01	53760.67	51696.51	54185.60	1.02	1.01	1.05
V_{sTx}	95673.36	96520.80	94402.11	98268.80	1.03	1.02	1.04
V_{sT}	240366.09	247061.77	241312.43	252396.80	1.05	1.02	1.05

Table 3 shows the solution for the case 2.

Table 3 Comparison of results to the case 2

Concept	TCF_1	TCF_2	TCF_3	RCF	Relationship 1	Relationship 2	Relationship 3
MF	a = 7.00 b_1 = 1.15 b_2 = 4.40	a = 7.50 b_1 = 1.65 b_2 = 3.50	a = 8.00 b_1 = 2.05 b_2 = 2.75	a = 8.40 b = 2.30	RCF/TCF_1	RCF/TCF_2	RCF/TCF_3

Table 3 Continued

M_{a1}	140.24	214.24	279.71	321.76	2.29	1.50	1.15
M_{a2}	1340.51	996.71	761.33	643.52	0.48	0.65	0.85
M_b	303.44	293.38	285.17	281.14	0.93	0.96	0.99
M_c	2800.80	2424.16	2130.10	1968.00	0.70	0.81	0.92
M_d	35.64	-316.54	-750.81	-1030.86	28.92	3.26	1.37
M_e	-279.10	-530.29	-914.03	-1171.43	4.20	2.21	1.28
$Ø_v V_{ff1}$	568.45	481.04	481.04	523.92	0.92	1.09	1.09
V_{ff1}	0	0	0	21.39	∞	∞	∞
$Ø_v V_{ff2}$	879.97	731.65	731.65	804.15	0.91	1.10	1.10
V_{ff2}	687.16	535.17	285.97	42.78	0.06	0.08	0.15
$Ø_v V_{fg}$	1149.75	1129.15	1244.37	1401.18	1.22	1.24	1.13
V_{fg}	1130.60	1055.48	954.77	866.86	0.77	0.82	0.91
$Ø_v V_{fh}$	2241.69	1682.21	1440.25	1401.18	0.63	0.83	0.97
V_{fh}	-1312.74	-1343.27	-1349.89	-1335.43	1.02	0.99	0.99
$Ø_v V_{fi}$	2935.39	1981.78	1549.70	1401.18	0.48	0.70	0.90
V_{fi}	0	203.42	508.45	632.57	∞	3.11	1.24
$Ø_v V_{cp11}$	6050.62	5081.19	5081.19	5555.97	0.92	1.09	1.09
$Ø_v V_{cp12}$	11095.23	8995.07	8995.07	10017.67	0.90	1.11	1.11
$Ø_v V_{cp13}$	3915.11	3287.82	3287.82	3595.04	0.92	1.09	1.09
V_{p1}	1332.91	1369.84	1368.26	1350.91	1.01	0.99	0.99
$Ø_v V_{cp21}$	10559.69	8779.74	8779.74	9649.85	0.91	1.10	1.10
$Ø_v V_{cp22}$	15604.82	12645.97	12645.97	14086.60	0.90	1.12	1.12
$Ø_v V_{cp23}$	6832.74	5681.00	5681.00	6244.02	0.90	1.10	1.10
V_{p2}	2804.62	2869.10	2866.69	2836.28	1.01	0.99	0.99
d	97	87	87	92	0.95	1.06	1.06
t	105	95	95	100	0.95	1.05	1.05
V_C	20.40	18.35	18.24	19.32	0.95	1.05	1.06
V_{sty}	65408.07	60459.75	59014.80	59623.20	0.91	0.99	1.01
V_{sby}	62142.99	57607.88	55932.24	59623.20	0.96	1.03	1.07
V_{sTy}	127551.06	118067.63	114947.04	119246.00	0.93	1.01	1.04
V_{stx}	37488.42	33320.70	33062.40	34985.30	0.93	1.05	1.06
V_{sbx}	47044.24	36099.19	37272.80	42906.50	0.91	1.19	1.15
V_{sTx}	84532.66	69419.89	70335.20	77891.80	0.92	1.12	1.11
V_{sT}	214922.92	187487.52	185282.24	197137.80	0.92	1.05	1.06

4. Results

Effects that govern the thickness of the combined footings are the moments, bending shear, and punching shear.

For case 1:

1) For the moments:

a) For the Relationship 1: The largest difference is presented on the *e-e* axis of 6.69 times greater the rectangular combined footing with respect to the trapezoidal combined footings, and the lowest percentage appears on the a_2-a_2 axis of the 75% for the rectangular combined footing with respect to the trapezoidal combined footings.

b) For the Relationship 2: The largest difference appears on the *e-e* axis of 1.62 times greater the rectangular combined footing with respect to the trapezoidal combined footings, and the lowest percentage is presented on the a_2-a_2 axis of the 88% for the rectangular combined footing with respect to the trapezoidal combined footings.

c) For the Relationship 3: The largest difference is presented on the a_2-a_2 axis of 1.14 times greater the rectangular combined footing with respect to the trapezoidal combined footings, and the lowest percentage appears on the *e-e* axis of the 72% for the rectangular combined footing with respect to the trapezoidal combined footings.

2) For the bending shear:

a) For the Relationship 1: The critical bending shear appears on the f_2-f_2 axis for the two footings, and the f_1-f_1 and *i-i* axes have not bending shear for the trapezoidal combined footing, because the f_1-f_1 and *i-i* axes are located outside of the footing.

b) For the Relationship 2: The critical bending shear appears on the f_2-f_2 axis for the two footings.

c) For the Relationship 3: The critical bending shear appears on the f_2-f_2 axis for the rectangular combined footing, and the *h-h* axis for the trapezoidal combined footing.

3) For the punching shear:

a) For the Relationship 1: The punching shear acting due to the boundary column for the trapezoidal combined footing is 5% than the rectangular combined footing, and for the inner column for the trapezoidal combined footing is 4% than the rectangular combined footing.

b) For the Relationship 2: The punching shear acting due to the boundary column and the inner column for the trapezoidal combined footing is 2% greater the rectangular combined footing.

c) For the Relationship 3: The punching shear acting due to the boundary column and the inner column for the trapezoidal combined footing have the 99% of the rectangular combined footing.

For case 2:

1) For the moments:

a) For the Relationship 1: The largest difference is presented on the *d-d* axis of 28.92 times greater the rectangular combined footing with respect to the trapezoidal combined footings, and the lowest percentage appears on the a_2-a_2 axis of the 48% for the rectangular combined footing with respect to the trapezoidal combined footings.

b) For the Relationship 2: The largest difference appears on the *d-d* axis of 3.26 times greater the rectangular combined footing with respect to the trapezoidal combined footings, and the lowest percentage is presented on the a_2-a_2 axis of the 65% for the rectangular combined footing with respect to the trapezoidal combined footings.

c) For the Relationship 3: The largest difference is presented on the *d-d* axis of 1.37 times greater the rectangular combined footing with respect to the trapezoidal combined footings, and the lowest percentage appears on the a_2-a_2 axis of the 85% for the rectangular combined footing with respect to the trapezoidal combined footings.

2) For the bending shear:

a) For the Relationship 1: The critical bending shear appears on the *g-g* axis for the trapezoidal combined footing, and the *h-h* axis for the rectangular combined footing, and the f_1-f_1 and *i-i* axes

have not bending shear for the trapezoidal combined footing, because the f_1-f_1 and *i*-*i* axes are located outside of the footing.

b) For the Relationship 2: The critical bending shear appears on the *g*-*g* axis for the trapezoidal combined footing, and the *h*-*h* axis for the rectangular combined footing, and the f_1-f_1 axis has not bending shear for the trapezoidal combined footing, because the f_1-f_1 axis is located outside of the footing.

c) For the Relationship 3: The critical bending shear appears on the *h*-*h* axis for the two footings, and the f_1-f_1 axis has not bending shear for the trapezoidal combined footing, because the f_1-f_1 axis is located outside of the footing.

3) For the punching shear:

a) For the Relationship 1: The punching shear acting due to the boundary column and the inner column for the trapezoidal combined footing is 1% greater the rectangular combined footing.

b) For the Relationship 2: The punching shear acting due to the boundary column and the inner column for the trapezoidal combined footing have the 99% of the rectangular combined footing.

c) For the Relationship 3: The punching shear acting due to the boundary column and the inner column for the trapezoidal combined footing have the 99% of the rectangular combined footing.

Materials used for the construction of the combined footings are the reinforcement steel and concrete.

For the case 1:

a) For the concrete: Greatest savings is presented in the relationship 1 and is of the 5% in the trapezoidal footing with respect to the rectangular footing.

b) For reinforcement steel: Greatest savings appears in the relationship 1 and is of the 5% in the trapezoidal footing with respect to the rectangular footing.

For the case 2:

a) For the concrete: Greatest savings appears in the relationship 3 and is of the 6% in the trapezoidal footing with respect to the rectangular footing.

b) For reinforcement steel: Greatest savings is presented in the relationship 3 and is of the 6% in the trapezoidal footing with respect to the rectangular footing.

5. Conclusions

The main findings of this research are as follows:

1. If the value "*a*" is increased: Moments acting on the a_1-a_1 axis is increased, and on the a_2-a_2, *b*-*b* and *c*-*c* axes are decreased, and on the *d*-*d* and *e*-*e* axes are increased in absolute value for the trapezoidal combined footings in the two cases.

2. If the value "*a*" is increased: Bending shear acting on the f_1-f_1, *h*-*h* and *i*-*i* axes are increased in absolute value, and on the f_2-f_2 and *g*-*g* axes are decreased for the trapezoidal combined footings in the two cases.

3. If the value "*a*" is increased: Punching shear acting due to the boundary column and the inner column are increased for the trapezoidal combined footings in the case 1, and for the case 2 the Relationship 2 is greater.

4. The trapezoidal combined footings are more economical than the rectangular combined footings agree to the construction materials (reinforcement steel and concrete).

The advantages of the trapezoidal combined footings on the rectangular combined footings using this methodology are:

The trapezoidal combined footings can be used for two boundaries of opposite sides (Luévanos-Rojas 2015a).

The rectangular combined footings can be used for one boundary of opposite sides (Luévanos-Rojas 2016b).

The suggestions for future research are:

1. Design of trapezoidal and rectangular combined footings using the optimization techniques (optimal cost).

2. Dimensioning and design for the trapezoidal and rectangular combined footings supported on another type of soil by example in totally cohesive soils (clay soils) and totally granular soils (sandy soils), the pressure diagram is not linear and should be treated differently.

References

ACI 318S-14 (2014), *Building Code Requirements for Structural Concrete and Commentary*, Committee 318, New York, U.S.A.

Agrawal, R. and Hora, M.S. (2012), "Nonlinear interaction behaviour of infilled frame-isolated footings-soil system subjected to seismic loading", *Struct. Eng. Mech.*, **44**(1), 85-107.

Bowles, J.E. (2001), *Foundation Analysis and Design*, McGraw-Hill, New York, U.S.A.

Calabera-Ruiz, J. (2000). *Calculo de Estructuras de Cimentación*, Intemac Ediciones, México.

Chen, W.R., Chen, C.S. and Yu, S.Y. (2011), "Nonlinear vibration of hybrid composite plates on elastic foundations", *Struct. Eng. Mech.*, **37**(4), 367-383.

Cure, E., Sadoglu, E., Turker, E. and Uzuner, B.A. (2014), "Decrease trends of ultimate loads of eccentrically loaded model strip footings close to a slope", *Geomech. Eng.*, **6**(5), 469-485.

Das, B.M., Sordo-Zabay, E. and Arrioja-Juárez, R. (2006), *Principios de Ingeniería de Cimentaciones*, Cengage Learning Latín América, México.

Dixit, M.S. and Patil K.A. (2013), "Experimental estimate of Nγ values and corresponding settlements for square footings on finite layer of sand", *Geomech. Eng.*, **5**(4), 363-377.

ErzÍn, Y. and Gul, T.O. (2013), "The use of neural networks for the prediction of the settlement of pad footings on cohesionless soils based on standard penetration test", *Geomech. Eng.*, **5**(6), 541-564.

González-Cuevas, O.M. and Robles-Fernández-Villegas, F. (2005), *Aspectos Fundamentales del Concreto Reforzado*, Limusa, México.

Guler, K. and Celep, Z. (2005), "Response of a rectangular plate-column system on a tensionless Winkler foundation subjected to static and dynamic loads", *Struct. Eng. Mech.*, **21**(6), 699-712.

Kurian, N.P. (2005), *Design of Foundation Systems*, Alpha Science Int'l Ltd, New York, U.S.A.

López-Chavarría, S., Luévanos-Rojas, A. and Medina-Elizondo, M. (2017), "Optimal dimensioning for the corner combined footings", *Adv. Comput. Des.*, **2**(2), 169-183.

Luévanos-Rojas, A. (2012a), "A mathematical model for dimensioning of footings square", *I.RE.C.E.*, **3**(4), 346-350.

Luévanos-Rojas, A. (2012b), "A mathematical model for the dimensioning of circular footings", *Far East J. Math. Sci.*, **71**(2), 357-367.

Luévanos-Rojas, A. (2013), "A mathematical model for dimensioning of footings rectangular", *ICIC Expr. Lett. Part B*: *Appl.*, **4**(2), 269-274.

Luévanos-Rojas, A., Faudoa-Herrera, J.G., Andrade-Vallejo, R.A. and Cano-Alvarez M.A. (2013), "Design of isolated footings of rectangular form using a new model", *J. Innov. Comput. I.*, **9**(10), 4001-4022.

Luévanos-Rojas, A. (2014a), "Design of isolated footings of circular form using a new model", *Struct. Eng. Mech.*, **52**(4), 767-786.

Luévanos-Rojas, A. (2014b), "Design of boundary combined footings of rectangular shape using a new model", *Dyna-Colomb.*, **81**(188), 199-208.

Luévanos-Rojas, A. (2015a), "A new mathematical model for dimensioning of the boundary trapezoidal combined footings", *J. Innov. Comput. I.*, **11**(4), 1269-1279.
Luévanos-Rojas, A. (2015b), "Design of boundary combined footings of trapezoidal form using a new model", *Struct. Eng. Mech.*, **56**(5), 745-765.
Luévanos-Rojas, A. (2016a), "A mathematical model for the dimensioning of combined footings of rectangular shape", *Rev. Tec. Fac. Ing. Univ.*, **39**(1), 3-9.
Luévanos-Rojas, A. (2016b), "A comparative study for the design of rectangular and circular isolated footings using new models", *Dyna-Colomb.*, **83**(196), 149-158.
Luévanos-Rojas, A. (2016c), "Un nuevo modelo para diseño de zapatas combinadas rectangulares de lindero con dos lados opuestos restringidos", *ALCONPAT*, **6**(2), 172-187.
Maheshwari, P. and Khatri, S. (2012), "Influence of inclusion of geosynthetic layer on response of combined footings on stone column reinforced earth beds", *Geomech. Eng.*, **4**(4), 263-279.
McCormac, J.C. and Brown, R.H. (2013), *Design of Reinforced Concrete*, John Wiley & Sons, Inc., México.
Mohamed, F.M.O., Vanapalli, S.K. and Saatcioglu, M. (2013), "Generalized Schmertmann Equation for settlement estimation of shallow footings in saturated and unsaturated sands", *Geomech. Eng.*, **5**(4), 363-377.
Orbanich, C.J., Dominguez, P.N. and Ortega, N.F. (2012), "Strenghtening and repair of concrete foundation beams whit fiber composite materials", *Mater. Struct.*, **45**, 1693-1704.
Orbanich, C.J. and Ortega, N.F. (2013), "Analysis of elastic foundation plates with internal and perimetric stiffening beams on elastic foundations by using finite differences method", *Struct. Eng. Mech.*, **45**(2), 169-182.
Punmia, B.C., Kr.-Jain, A. and Kr.-Jain, A. (2007), *Limit State Design of Reinforced Concrete*, Laxmi Publications (P) Limited, New York, U.S.A.
Rad, A.B. (2012), "Static response of 2-D functionally graded circular plate with gradient thickness and elastic foundations to compound loads", *Struct. Eng. Mech.*, **44**(2), 139-161.
Shahin, M.A. and Cheung, E.M. (2011), "Stochastic design charts for bearing capacity of strip footings", *Geomech. Eng.*, **3**(2), 153-167.
Smith-Pardo, J.P. (2011), "Performance-based framework for soil-structure systems using simplified rocking foundation models", *Struct. Eng. Mech.*, **40**(6), 763-782.
Tomlinson, M.J. (2008), *Cimentaciones, Diseño y Construcción*, Trillas, México.
Uncuoglu, E. (2015), "The bearing capacity of square footings on a sand layer overlying clay", *Geomech. Eng.*, **9**(3), 287-311.
Varghese, P.C. (2009), *Design of Reinforced Concrete Foundations*, PHI Learning Pvt. Ltd., New York, U.S.A.
Zhang, L., Zhao, M.H., Xiao, Y. and Ma, B.H. (2011), "Nonlinear analysis of finite beam resting on Winkler with consideration of beam-soil interface resistance effect", *Struct. Eng. Mech.*, **38**(5), 573-592.

CC